THE JOURNAL OF PHYSICAL CHEMISTRY Letters

Letter

pubs.acs.org/JPCL

Multiscale Modeling of Plasmon-Enhanced Power Conversion Efficiency in Nanostructured Solar Cells

Lingyi Meng,[†] ChiYung Yam,*[,‡,§] Yu Zhang,[§,∥] Rulin Wang,[‡] and GuanHua Chen[§]

[†]Collaborative Innovation Center of Chemistry for Energy Materials, Xiamen University, Xiamen 361005, P. R. China

[‡]Beijing Computational Science Research Center, Beijing 100094, P. R. China

[§]Department of Chemistry, The University of Hong Kong, Pokfulam Road, Pokfulam, Hong Kong

[∥]Center for Bio-inspired Energy Science, Northwestern University, Evanston, Illinois 60208, United States

ABSTRACT: The unique optical properties of nanometallic structures can be exploited to confine light at subwavelength scales. This excellent light trapping is critical to improve light absorption efficiency in nanoscale photovoltaic devices. Here, we apply a multiscale quantum mechanics/electromagnetics (QM/EM) method to model the current−voltage characteristics and optical properties of plasmonic nanowire-based solar cells. The QM/EM method features a combination of first-principles quantum mechanical treatment of the photoactive component and classical description of electromagnetic environment. The coupled optical-electrical QM/EM simulations demonstrate a dramatic enhancement for power conversion efficiency of nanowire solar cells due to the surface plasmon effect of nanometallic structures. The improvement is attributed to the enhanced scattering of light into the photoactive layer. We further investigate the optimal configuration of the nanostructured solar cell. Our QM/EM simulation result demonstrates that a further increase of internal quantum efficiency can be achieved by scattering light into the n-doped region of the device.

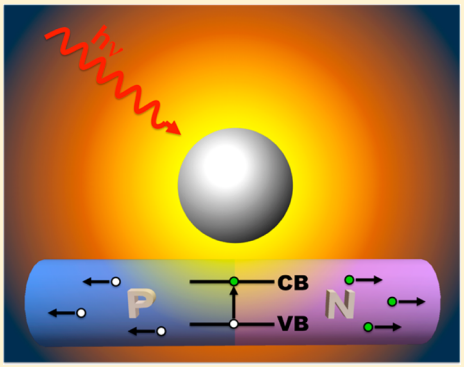

Photovoltaic technology converting solar energy into electricity is being recognized as an essential component of future renewable energy production.[1] This in principle can provide an unlimited amount of energy to the world. For decades, silicon has been the material of choice and has dominated the photovoltaics market. Power conversion efficiencies (PCE) of over 25% have been realized in silicon-based solar cells.[2] Due to the low-absorbing nature of silicon, cell thickness on the order of a few hundred micrometers is usually required to achieve high efficiency, which constitutes the major cost component of photovoltaic modules. For large-scale implementation of photovoltaic technology, the cost of photovoltaic modules has to be further reduced and tremendous amount of effort has been made to reduce the material usage. Nanostructured photovoltaic devices based on a variety of semiconductor materials may offer a viable way toward this goal and thereby have attracted increasing attention. In particular, nanowire-based solar cells have been recognized as promising candidates for third-generation photovoltaics. Recent studies demonstrated the ability of nanowire-based solar cells to achieve high PCE, which breaks the traditional Shockley−Queisser limit.[3,4] Although the shrinkage of device dimensions in nanowire solar cells is beneficial for the reduction of active material required and the charge carrier collection, it leads to poor optical absorption.[5]

Advanced antireflection and light trapping schemes had been developed to overcome the low optical absorption problems. By integration of photonic nanostructures, it had been demonstrated that light could be effectively trapped within the photoactive layer,[5] thereby increase the optical path length.[6−8] The increase of optical path length not only enhances optical absorption but also allows the use of a larger variety of materials, including those with lower abundance and carrier diffusion length. An effective method for achieving light confinement in nanostructured solar cells is the use of metallic nanostructures that support localized surface plasmon resonances.[5] The field of plasmonics is developing rapidly and has emerged as a new area for materials and device research. Surface plasmons refer to the collective excitations of conduction electrons at the interface between a metal and a dielectric, resulting in strong field localization.[9] By proper engineering of these nanostructures (e.g., materials, geometries, sizes, and geometrical arrangements), light can be concentrated and scattered into the photoactive layer, thereby enhancing the optical absorption of solar cells.[10] Here, the metallic nanostructures act as an antenna that converts incident energy from sunlight to localized surface plasmon modes. Experimentally, enhanced PCEs have been demonstrated for organic solar cells doped with silver nanoparticles due to associated plasmonic near-field effects.[11,12] Lindquist et al. improved absorption efficiency of organic solar cells using a plasmonic nanocavity array formed by the local field enhancement of a

Received: September 1, 2015
Accepted: October 21, 2015
Published: October 21, 2015

DOI: 10.1021/acs.jpclett.5b01913
J. Phys. Chem. Lett. 2015, 6, 4410−4416

patterned metal anode.[13] Plasmonic enhancements have also been applied to inorganic solar cells[14] and dye-sensitized solar cells.[15,16]

Despite its success, many of the underlying physical mechanisms have not been studied systematically. In particular, most of the theoretical descriptions of plasmonic solar cells neglected the coupled optical−electrical processes. These studies involved only electromagnetic modeling of optical absorption with the assumptions of ideal carrier transport.[17] On the other hand, there exist classical methods based on the dynamic Monte Carlo approach[18,19] and the macroscopic continuum device model[20,21] to study the performance of solar cells. Up until recently, there have been few theoretical works carried out to study the multiphysics process in plasmonic solar cells.[22−24] However, these approaches rely on many empirical parameters, including carrier mobilities, dielectric functions, and electron−hole generation and recombination rates. To predict and, hence, optimize the performance of plasmonic solar cells, accurate descriptions of the optical and electronic properties of these nanostructures are inevitable.

Recently, we have developed a quantum mechanical method based on nonequilibrium Green's function (NEGF) techniques to describe electron−photon interactions in nanoscale systems.[25] The method has been applied to study the performance of nanowire-based photovoltaic devices. Nevertheless, plasmonic solar cells involve processes that couple light both with nanometallic structures and semiconducting photoactive layers. A full quantum mechanical description of the entire system is thus computational challenging.[26] There have been some hybrid approaches proposed to study plasmon/molecule systems.[27−29] In this paper, we applied the QM/EM method[30−33] to model the current−voltage characteristics and optical properties of plasmonic nanowire-based solar cells. Here, classical electrodynamics of a silver nanoparticle is directly coupled to quantum mechanical simulations of silicon-nanowire-based *p-n* junctions. We found a dramatic enhancement in PCE of nanowire solar cells due to the near-field effect of plasmonic structures. In particular, we found that an increase of ∼70% in internal quantum efficiency (IQE) by coupling light into the n-doped part of the device as compared to the p-doped counterpart.

We consider a photovoltaic device comprising of a metallic nanoparticle and a nanostructured solar cell. The multiscale QM/EM method combines a classical electrodynamics description of plasmon excitation in the nanoparticle and a quantum mechanical treatment of optical and electrical processes in the photoactive component of the device, which is identified as the QM region. Classical electrodynamics simulation of the whole device is first performed based on the finite volume method (FVM) to determine its electromagnetic properties.[31,32,34,35] The device is discretized into small rectangular building blocks each characterized by a frequency-dependent dielectric permittivity, ε, and a magnetic permeability, μ, where these material properties are assumed to be uniform inside each building block. A source generating continuous plane wave electromagnetic field at particular frequency is modeled by invoking an infinite current sheet on the surface perpendicular to the propagation direction.[36] This incident field is irradiated on the system and interacts with the nanoparticle, creating an enhanced surface local field. The boundary surfaces are truncated with Mur first-order absorbing boundary conditions to avoid reflections.[37,38] In addition, a static bias potential is applied at the boundary where electrical contacts of the solar cell are located and a standard drift-diffusion model is adopted to describe the semiconductors in the device. The Maxwell equations in potential representation[32]

$$\nabla\cdot[\varepsilon(-\nabla V - i\omega\vec{A})] - \rho = 0 \tag{1}$$

$$\nabla\times\left[\frac{1}{\mu}(\nabla\times\vec{A})\right] - [\vec{J} + i\omega(\varepsilon(-\nabla V - i\omega\vec{A}))] = 0 \tag{2}$$

are then solved in the frequency domain to obtain the scalar potential V, vector potential $\vec{A}$, and current density $\vec{J}$. ρ denotes the charge density. ω is the frequency. Coulomb gauge is adopted and thus $\nabla\cdot\vec{A} = 0$. The scalar potential V and vector potential $\vec{A}$ are related to electric field $\vec{E}$ and the magnetic induction $\vec{B}$ as

$$\vec{B} = \nabla\times\vec{A} \tag{3}$$

$$\vec{E} = -\nabla V - i\omega\vec{A} \tag{4}$$

The electrodynamics of the device is coupled with a quantum mechanical treatment of the photoactive component based on NEGF method.[25] The scalar potential V and vector potential $\vec{A}$ in the QM region are employed as input for the subsequent quantum mechanical simulations. Specifically, under Coulomb gauge, the interaction of electrons and photons is given by

$$H_{\mathrm{ep}} = \frac{e}{m}\vec{A}\cdot\vec{p} \tag{5}$$

Here, $\vec{A}$ is the external electromagnetic vector potential obtained from the classical electrodynamics simulations. Equation 5 describes the coupling between photons and electrons and gives rise to photoexcitation of electron−hole pairs and their radiative recombination. $\vec{p}$ is the electronic momentum, e and m are the elementary charge and electron mass, respectively. In addition, the static potential V at the surfaces enclosing the QM region is employed as boundary condition to solve Poisson's equation for the electrostatics inside. In our previous work, we neglected the spatial distribution of vector potential $\vec{A}$ because the systems studied are much smaller compared to the wavelength of external field.[25] The vector potential thereby is assumed to be constant over the system. However, due to the subwavelength optical confinement nature of surface plasmons, the external electromagnetic field can be scattered below the diffraction limit. We therefore explicitly consider the spatial dependence of vector potential in this work. The vector potential, $\vec{A}$ obtained from classical electrodynamics simulations is expressed in second quantized form

$$\vec{A}(\mathbf{r}, t) = \vec{a}\left(\frac{\hbar\sqrt{\tilde{\mu}\tilde{\varepsilon}}}{2N\omega\varepsilon c}I_\omega\right)^{1/2}(be^{-i\omega t} + b^\dagger e^{i\omega t}) \tag{6}$$

where $\tilde{\mu}$ and $\tilde{\varepsilon}$ are relative magnetic and dielectric constants, respectively; $\hbar$ is the reduced Planck constant; c is velocity of electromagnetic field; N is the number of photons following the Bose−Einstein statistics; I_ω is the corresponding photon flux, which is defined as the number of photons per unit time per unit area. $\vec{a}$ gives the polarization direction of $\vec{A}$. b and $b^\dagger$ are the annihilation and creation operators of photons, respectively. Applying perturbation theory, the electron−photon interaction in eq 5 can be expressed through self-energies $\sum_{\mathrm{ep}}^{<,>}$,[25,39]

DOI: 10.1021/acs.jpclett.5b01913
J. Phys. Chem. Lett. 2015, 6, 4410−4416

$$\Sigma_{ep}^{<,>}(E) = M[NG^{<,>}(E \mp \hbar\omega) + (N+1)G^{<,>}(E \pm \hbar\omega)]M \tag{7}$$

where M is the electron−photon coupling matrix, and its matrix elements are given by

$$M_{\mu\nu} = e\left(\frac{\hbar\sqrt{\tilde{\mu}\tilde{\varepsilon}}}{2N\omega\varepsilon c}I_\omega\right)^{1/2}\vec{a}\cdot\langle\mu|\frac{\vec{p}}{m}|\nu\rangle \tag{8}$$

and $G^<(E)$ and $G^>(E)$ correspond to lesser and greater Green's function, respectively, and are given by

$$G^{<,>}(E) = G^r(E)[\sum_\alpha \Sigma_\alpha^{<,>}(E) + \Sigma_{ep}^{<,>}(E)]G^a(E) \tag{9}$$

where $\sum_\alpha^{<,>}(E)$ are the self-energies accounting for the coupling to the αth electrode. $G^r(E)$ and $G^a(E)$ are the retarded and advanced Green's functions, respectively. Because the system studied in this work is small compared to the coherence length, electrons are assumed to pass through the device without being scattered by phonons. In fact, there are experimental works demonstrate that coherence length of carriers in nanowires can be much longer even at room temperature due to reduced backscattering.[40] Thus, the electron−phonon coupling and its decoherence effect are neglected to reduce the computational costs. Finally, the resulting Green's functions and self-energies are used to evaluate the current at electrode α,

$$J_\alpha = \frac{2e}{\hbar}\int\frac{dE}{2\pi}\mathrm{Tr}[\Sigma_\alpha^<(E)G^>(E) - \Sigma_\alpha^>(E)G^<(E)] \tag{10}$$

Here, the first term in the integrand is interpreted as the rate of electrons leaving from system to the αth electrode and the second term corresponds to the rate of electrons entering the system from the αth electrode. In this work, the effect of electrical properties of the solar cell on the optical response of the metal nanoparticle is assumed to be small; thus, the back coupling of quantum simulations on the electrodynamics is not considered. In general, this can be done by invoking current from eq 10 as input to the electrodynamics simulations.[33] Finally, the $J-V$ characteristics and, hence, PCE of the solar cell can be determined by varying the bias potential at the electrical contacts of the cell.

We apply the multiscale QM/EM method to model a plasmonic photovoltaic device and study the effect of optical enhancement on its PCE. The system contains a 10 nm diameter silver nanosphere and a silicon nanowire (SiNW) as the photoactive component of the solar cell as shown in Figure 1. The nanosphere is located 2 nm above the SiNW, so the quantum tunneling between them can be neglected.[41−43] The entire simulation box with a dimension of 42 × 30 × 30 nm^3 is discretized into small building blocks with the minimum building block size is 0.016 nm^3. Each building block is characterized by ε and μ values based on its constituent material. The values of ε and μ for silver and silicon are obtained from experiment[31,44] and ε = 1 for the surrounding medium. An infinite current sheet is applied on the surface at y = −15 nm to provide a continuous incident light source with irradiance of 1000 W/m^2 propagating in y direction.

The interaction of incident light with the nanosphere leads to surface plasmon excitations. Figure 1 plots field strength distribution displaying enhancement of local electromagnetic field around surface of the silver nanosphere. The field is highly localized at the nanosphere and decays rapidly away from the metal/dielectric interface. Figure 2a shows the enhancement

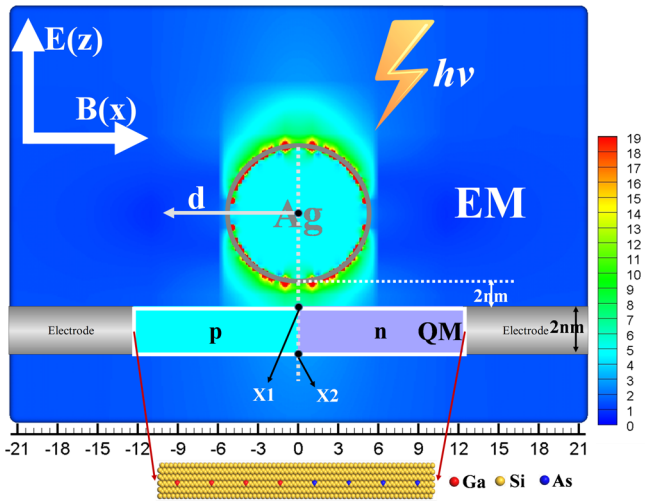

Figure 1. Schematic diagram of a plasmonic photovoltaic device for a coupled optical−electrical QM/EM simulation. The system contains a silver nanosphere and is placed 2 nm above a silicon nanowire. The diagram is overlaid with the contour of surface localized field generated by the silver nanosphere.

factor of electric field strength with respect to incident light frequencies ω at two given positions marked in Figure 1. The enhancement factor of electric field strength is defined as

$$\Gamma(\omega) = \left|\frac{\vec{E}_{sca}(\omega)}{\vec{E}_0(\omega)}\right| \tag{11}$$

where $\vec{E}_{sca}(\omega)$ is the scattered electric field and $\vec{E}_0(\omega)$ the incident field. At both positions X1 and X2, a feature peak centered at around 3.4 eV is observed in Figure 2a, which corresponds to resonant excitation of the dipole surface plasmon of the silver nanosphere.[27,29] It is expected that the field strength should decrease as distance from the silver nanosphere increases, showing the evanescence nature of surface plasmons. Figure 2b−d show the field distributions in the QM region where the photoactive component of the device located. The incident light frequency is set at 3.0 and 3.4 eV, which correspond to the off-resonance and on-resonance frequencies of the silver nanosphere, respectively. The incident light has a polarization direction along the z axis. As manifested from the simulated field distribution, the optical confinement nature of the silver nanosphere concentrates light into subwavelength region near its surface. At on-resonance frequency of 3.4 eV, a maximum field enhancement of 7 is found near the surface of the SiNW and decays away from the nanosphere. As shown in Figure 2b, the enhancement reduces substantially as light frequency moves away from resonance. By directing more incident light into the photoactive component, the optical absorption capability can be significantly increased.

The QM region encloses a SiNW of dimension of 2 × 2 × 25 nm^3. The atomistic model contains 6656 atoms and is oriented in [110] direction. The surface of SiNW is passivated with hydrogen atoms to eliminate dangling bond. To form a p-n junction, four Ga and four As atoms are explicitly doped in the system, giving a doping concentration of about 8.0 × 10^{19} cm^{-3} and a built-in potential of about 1.13 V across the junction. Experimentally, growth of single-crystal silicon nanowires with diameters approaching molecular dimensions has been reported.[45] In addition, nanowires with widths down to 4 nm have been fabricated by means of lithography.[46] This top-down

DOI: 10.1021/acs.jpclett.5b01913
J. Phys. Chem. Lett. 2015, 6, 4410−4416

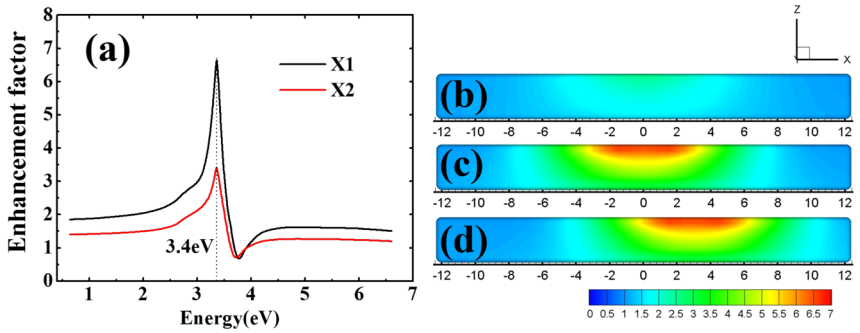

Figure 2. (a) Enhancement factor of electric field strength near the metallic nanosphere at different observation points marked in Figure 1. Contour plot of field strength enhancement in the QM region (b) with photon energy = 3.0 eV and d = 0 nm, (c) photon energy = 3.4 eV and d = 0 nm, and (d) photon energy = 3.4 eV and d = 3 nm.

approach shows the possibility of device fabrication based on the $p-n$ junction nanowire used in this work.

To describe electronic structure of the silicon nanowire, we employ a density functional tight-binding (DFTB) Hamiltonian. DFTB is an approximate density functional theory method, based on the second-order expansion of the Kohn–Sham energy functional with respect to a reference density. In this work, we have used the "pbc-0–3" parameter set for silicon which has been successfully applied to study silicon clusters.[47] For the full details of DFTB, we refer the interested readers to ref 48. We first simulate the photocurrent of the device at zero bias voltage and ambient temperature is assumed. The dependence of short circuit current J_{sc} versus incident light frequency is shown in Figure 3. Obviously, J_{sc} roughly correlates

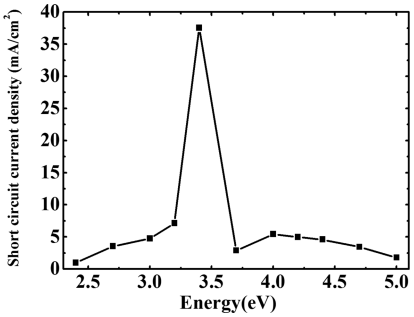

Figure 3. Short-circuit currents J_{sc} of the plasmonic solar cell versus incident photon energy.

with the local field enhancement as plotted in Figure 2a. Upon light illumination, an electron–hole pair is generated in the nanowire when a photon is absorbed. Due to the built-in potential of $p-n$ junction, electrons flow from the p-doped region to the n-doped region, whereas holes transport in the opposite direction, resulting in a photocurrent. At resonance frequency, the increased photon flux due to local field enhancement generated by surface plasmons substantially improves the optical absorption in the photoactive component. The enhanced absorption is followed by a higher generation rate of electron–hole pairs and results in an increase of photocurrent. To investigate the effect of polarization direction, we also simulate J_{sc} of the plasmonic device illuminated with light polarized in x direction at resonance frequency. When incident light is polarized in x direction, the enhanced field is mainly distributed in the horizontal positions near the surface of nanosphere. Thus, the total irradiance on the nanowire is substantially reduced and the plasmonic enhanced J_{sc} is increased only by 37%. In contrast, a 15 times enhancement of J_{sc} is obtained when light is polarized in z direction.

With the enhancement of J_{sc}, it is interesting to study the actual device performance. In the simulations, the plasmon resonance frequency of 3.4 eV is chosen, which shows the largest optical enhancement. The light intensity at the selected frequency is about one-third of the average light intensity in the visible part of AM 1.5G solar spectrum. To tune the plasmon resonance wavelength to the visible region, plasmonic structures with different materials, shapes, sizes, and geometrical arrangements can be used. Experimentally, this has been adopted for broadband plasmonic absorption enhancements in realistic devices.[49] The $J-V$ characteristics of the photovoltaic device are shown in Figure 4. For comparison, the

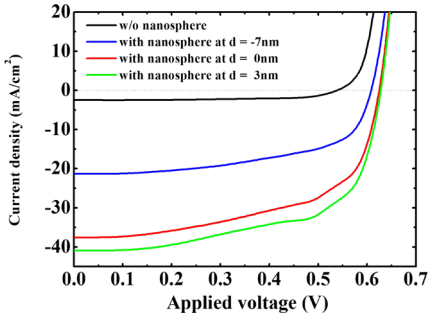

Figure 4. $J-V$ characteristics of SiNW solar cell illuminated by the monochromatic light of frequency 3.4 eV. Black line: without nanosphere. Red line: with nanosphere at d = 0 nm. Blue line: with nanosphere and d = −7 nm. Green line: with nanosphere at d = 3 nm.

$J-V$ characteristics of a reference device without silver nanoparticles are also plotted. The devices are under illumination of monochromatic light with frequency of 3.4 eV. Summarized in Table 1 are quantitative details of the device

Table 1. Electrical Performance Characteristics of Plasmonic SiNW Solar Cell Compared with a Reference Cell without Silver Nanospheres

	J_{SC} (mA/cm²)	V_{OC} (V)	fill factors	PCEs (%)
without nanosphere	2.49	0.54	0.65	0.9
10 nm nanosphere at d = 0 nm	37.54	0.62	0.6	13.9
10 nm nanosphere at d = −7 nm	21.27	0.6	0.59	7.5
10 nm nanosphere at d = 3 nm	40.92	0.63	0.62	16.1

DOI: 10.1021/acs.jpclett.5b01913
J. Phys. Chem. Lett. 2015, 6, 4410–4416

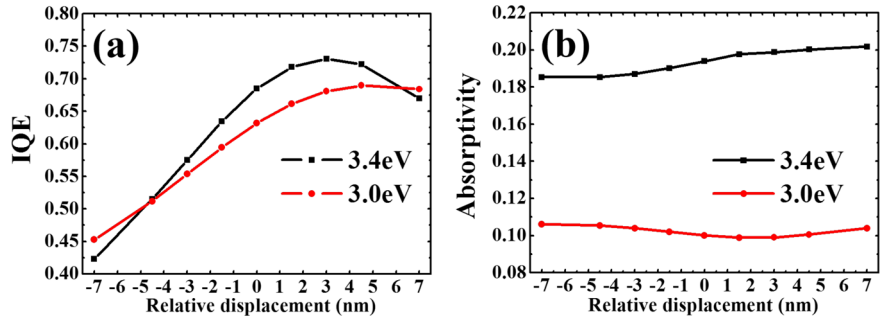

Figure 5. Dependency of IQE (a) and absorptivity (b) on the displacement d (defined as in Figure 1). Black line: illuminated light frequency of 3.4 eV. Red line: illuminated light frequency of 3.0 eV.

performance. Overall, the reference device demonstrates a PCE of 0.9%, J_{sc} of 2.49 mA/cm^2, open-circuit voltage (V_{oc}) of 0.54 V, and a fill factor (FF) of 0.65. Meanwhile, in the presence of silver nanosphere (placed in the middle), the device shows a PCE of 13.9%, J_{sc} of 37.54 mA/cm^2, V_{oc} of 0.62 V, and a FF of 0.60. In comparison, the plasmonic device shows substantial improvements to J_{sc} and PCE, both exceeds 15 times. However, it should be noted that although the nanosphere used in the simulation leads to remarkable improvements of PCE, it possesses only a single resonant peak, which limits the PCE enhancement to a narrow range of the solar spectrum. To further improve the performance, nanoparticle of various shapes can be used for broadband plasmonic absorption.[49]

In previous section, we demonstrate a dramatic improvement of device performance due to strong local field enhancement of plasmonic effect. The subwavelength optical confinement of surface plasmons has lead us to study spatial dependence of enhanced electromagnetic field on the device performance. We displace the nanosphere in the lateral direction as shown in Figure 1. The enhanced field distribution in QM region for d = 3 nm is shown in Figure 2d, which is essentially a rigid shift following the displacement of nanosphere. We further investigate in Figure 5 the dependence of optical absorption and IQE on the nanosphere displacement at both on-resonance and off-resonance frequencies. The results at both frequencies show that although absorption exhibits a weak dependence on the nanosphere displacement, there is a maximum of about 70% increase in IQE when the nanosphere is placed near the n-doped region compared to the p-doped region as shown in Figure 5a. Physically, upon absorption of a photon, an electron−hole pair is generated. The results shown in Figure 5b imply a similar carrier generation rate when the nanosphere is placed at different positions. The electron−hole pair then either separates over the built-in potential in the space charge region of the p−n junction or recombines. In the former case, electrons and holes are collected at opposite electrodes, a process that gives rise to photocurrent. The latter results in energy loss through radiative decay. IQE describes the ratio of the number of charge carriers collected to the number of photons absorbed by the solar cell. From our simulations, a higher IQE is found when most electron−hole pairs are generated at the n-doped side. Thus, we expect carriers generated there to diffuse more effectively to electrodes and, hence, with a lower recombination rate compared to those generated at the p-doped counterpart. We further calculate the bandstructures using DFTB method for a p-doped and an n-doped silicon nanowires separately and extract effective masses of the minority carriers in each case. Our results (not shown here) show that effective mass of minority carriers in p-doped SiNW is about 33% larger than that in n-doped SiNW. This suggests that mobile carriers in n-doped silicon have a longer lifetime and diffusion length, which is in agreement with previous experiments.[50−52] Figure 4 shows also the J−V characteristics when the nanosphere is placed at different positions. Due to the difference in IQE, a further enhancement in PCE of the device is observed when the nanosphere is positioned at d = 3 nm, whereas the performance degrades when the nanosphere is positioned at d = −7 nm (see also Table 1).

In conclusion, we apply a multiscale QM/EM method to study the performance of plasmonic solar cells. Combining a classical description of plasmonic nanostructure and quantum mechanical treatment of photoactive component, we determine the device performance and optical parameters of a SiNW solar cell. Through incorporating a silver nanosphere, we demonstrate enhancement of light scattering into the photoactive component due to surface plasmon excitation, and increased optical absorption leads to a dramatic improvement of the PCE of a SiNW solar cell. In addition, the spatial dependence of the local enhanced field is investigated and IQE can be improved by scattering light into the n-doped region of the device, leading to the longer lifetime and diffusion lengths of mobile carriers.

Nanowire solar cells can be made from individual nanowires or arrays. The model used in this work enables studies of fundamental processes and understanding transport, doping, and charge separation properties in nanowire-based solar cells. The setup in this work can be realized in experiments by putting the nanometallic structures in close proximity to nanowires lying flat on a substrate or in between nanowires in cases of nanowire array solar cells. In both cases, with light shining from the top, the nanometallic structures are expected to effectively confine light into the photoactive unit. At the device level, there are many factors affecting the performance of solar cells. Many further studies of plasmonic solar cells can be carried out, including losses of light due to multiple plasmonic particles and light trapping effect in array geometries. The multiscale approach presented in this work is well suited to address these issues.

The present work demonstrates the multiscale QM/EM method as an efficient simulation tool to describe the coupled optical−electrical processes in plasmonic devices. This is useful for understanding the mechanism of their energy conversion and helpful for improving the design of next generation solar cells. The QM/EM method can be extended to include self-consistently the back coupling of quantum mechanical

DOI: 10.1021/acs.jpclett.5b01913
J. Phys. Chem. Lett. 2015, 6, 4410−4416

simulations on the optical properties of metallic nanoparticle. This extension would also be useful for studying plasmonic light-emitting devices.

AUTHOR INFORMATION

Corresponding Author

*E-mail: yamcy@csrc.ac.cn.

Notes

The authors declare no competing financial interest.

ACKNOWLEDGMENTS

The authors would like to thank Zhongqun Tian of Xiamen University and Zhigang Shuai of Tsinghua University for helpful discussions. The financial support from the National Natural Science Foundation of China (21403176 (L.Y.M.), 21322306(C.Y.Y.), 21273186(G.H.C., C.Y.Y.)), National Basic Research Program of China (No. 2014CB921402 (C.Y.Y.)), the University Grant Council (AoE/P-04/08(G.H.C., C.Y.Y.)), and the University of Hong Kong (UDF on Fast Algorithm) is gratefully acknowledged.

REFERENCES

(1) Chu, S.; Majumdar, A. Opportunities and Challenges for a Sustainable Energy Future. *Nature* **2012**, *488*, 294−303.

(2) Green, M. A.; Emery, K.; Hishikawa, Y.; Warta, W.; Dunlop, E. D. Solar Cell Efficiency Tables. *Prog. Photovoltaics* **2015**, *23*, 1−9.

(3) Wallentin, J.; Anttu, N.; Asoli, D.; Huffman, M.; Åberg, I.; Magnusson, M. H.; Siefer, G.; Fuss-Kailuweit, P.; Dimroth, F.; Witzigmann, B.; et al. InP Nanowire Array Solar Cells Achieving 13.8% Efficiency by Exceeding the Ray Optics Limit. *Science* **2013**, *339*, 1057−1060.

(4) Krogstrup, P.; Jørgensen, H. I.; Heiss, M.; Demichel, O.; Holm, J. V.; Aagesen, M.; Nygard, J.; Morral, A. F. i. Single-Nanowire Solar Cells Beyond the Shockley−Queisser Limit. *Nat. Photonics* **2013**, *7*, 306−310.

(5) Atwater, H. A.; Polman, A. Plasmonics for Improved Photovoltaic Devices. *Nat. Mater.* **2010**, *9*, 205−213.

(6) Garnett, E.; Yang, P. Light Trapping in Silicon Nanowire Solar Cells. *Nano Lett.* **2010**, *10*, 1082−1087.

(7) Wang, W.; Wu, S.; Reinhardt, K.; Lu, Y.; Chen, S. Broadband Light Absorption Enhancement in Thin-Film Silicon Solar Cells. *Nano Lett.* **2010**, *10*, 2012−2018.

(8) Kelzenberg, M. D.; Boettcher, S.; Petykiewicz, J. A.; Turner-Evans, D. B.; Putnam, M. C.; L.Warren, E.; Spurgeon, J. M.; Briggs, R. M.; Lewis, N. S.; Atwater, H. A. Enhanced Absorption and Carrier Collection in Si Wire Arrays for Photovoltaic Applications. *Nat. Mater.* **2010**, *9*, 239−244.

(9) Sundaramurthy, A.; Crozier, K. B.; Kino, G. S.; Fromm, D. P.; Schuck, P. J.; Moerner, W. E. Field Enhancement and Gap-Dependent Resonance in a System of Two Opposing Tip-to-Tip Au Nanotriangles. *Phys. Rev. B: Condens. Matter Mater. Phys.* **2005**, *72*, 165409.

(10) Chou, C.-H.; Chen, F.-C. Plasmonic Nanostructures for Light Trapping in Organic Photovoltaic Devices. *Nanoscale* **2014**, *6*, 8444−8458.

(11) Rand, B. P.; Peumans, P.; Forrest, S. R. Long-Range Absorption Enhancement in Organic Tandem Thin-Film Solar Cells Containing Silver Nanoclusters. *J. Appl. Phys.* **2004**, *96*, 7519−7526.

(12) Kim, S.-S.; Na, S.-I.; Jo, J.; Kim, D.-Y.; Nah, Y.-C. Plasmon Enhanced Performance of Organic Solar Cells Using Electrodeposited Ag Nanoparticles. *Appl. Phys. Lett.* **2008**, *93*, 073307.

(13) Lindquist, N. C.; Luhman, W. A.; Oh, S.-H.; Holmes, R. J. Plasmonic Nanocavity Arrays for Enhanced Efficiency in Organic Photovoltaic Cells. *Appl. Phys. Lett.* **2008**, *93*, 123308.

(14) Derkacs, D.; Lim, S. H.; Matheu, P.; Mar, W.; Yu, E. T. Improved Performance of Amorphous Silicon Solar Cells Via Scattering from Surface Plasmon Polaritons in Nearby Metallic Nanoparticles. *Appl. Phys. Lett.* **2006**, *89*, 093103.

(15) Brown, M. D.; Suteewong, T.; Kumar, R. S. S.; D'Innocenzo, V.; Petrozza, A.; Lee, M. M.; Wiesner, U.; Snaith, H. J. Plasmonic Dye-Sensitized Solar Cells Using Core-Shell Metal-Insulator Nanoparticles. *Nano Lett.* **2011**, *11*, 438−445.

(16) Standridge, S. D.; Schatz, G. C.; Hupp, J. T. Distance Dependence of Plasmon-Enhanced Photocurrent in Dye-Sensitized Solar Cells. *J. Am. Chem. Soc.* **2009**, *131*, 8407−8409.

(17) Munday, J. N.; Atwater, H. A. Large Integrated Absorption Enhancement in Plasmonic Solar Cells by Combining Metallic Gratings and Antireflection Coatings. *Nano Lett.* **2011**, *11*, 2195−2201.

(18) Meng, L.; Shang, Y.; Li, Q.; Li, Y.; Zhan, X.; Shuai, Z.; Kimber, R. G. E.; Walker, A. B. Dynamic Monte Carlo Simulation for Highly Efficient Polymer Blend Photovoltaics. *J. Phys. Chem. B* **2010**, *114*, 36−41.

(19) Meng, L.; Wang, D.; Li, Q.; Yi, Y.; Bredas, J.-L.; Shuai, Z. An Improved Dynamic Monte Carlo Model Coupled with Poisson Equation to Simulate the Performance of Organic Photovoltaic Devices. *J. Chem. Phys.* **2011**, *134*, 124102.

(20) Shang, Y.; Li, Q.; Meng, L.; Wang, D.; Shuai, Z. Device Simulation of Low-Band Gap Polymer Solar Cells: Influence of Electron-Hole Pair Dissociation and Decay Rates on Open-Circuit Voltage. *Appl. Phys. Lett.* **2010**, *97*, 143511.

(21) Shuai, Z.; Meng, L.; Jiang, Y. Theoretical Modeling of the Optical and Electrical Processes in Organic Solar Cells. In *Progress in High-Efficient Solution Process Organic Photovoltaic Devices*; Springer: Berlin/Heidelberg, 2015; Vol. *130*, p 101−142.

(22) In, S.; Mason, D. R.; Lee, H.; Jung, M.; Lee, C.; Park, N. Enhanced Light Trapping and Power Conversion Efficiency in Ultrathin Plasmonic Organic Solar Cells: A Coupled Optical-Electrical Multiphysics Study on the Effect of Nanoparticle Geometry. *ACS Photonics* **2015**, *2*, 78185.

(23) Vervisch, W.; Riviére, G.; Vedraine, S.; Biondo, S. p.; Torchio, P.; Duché, D.; Simon, J.-J.; Escoubas, L. Optical-Electrical Simulation of Organic Solar Cells: Influence of Light Trapping by Photonic Crystal and ZnO Spacer on Electrical Characteristics. *J. Appl. Phys.* **2012**, *111*, 094506.

(24) Li, X.; Hylton, N. P.; Giannini, V.; Lee, K.-H.; Ekins-Daukes, N. J.; Maier, S. A. Bridging Electromagnetic and Carrier Transport Calculations for Three-Dimensional Modelling of Plasmonic Solar Cells. *Opt. Express* **2011**, *19*, A888.

(25) Zhang, Y.; Meng, L.; Yam, C.; Chen, G. Quantum-Mechanical Prediction of Nanoscale Photovoltaics. *J. Phys. Chem. Lett.* **2014**, *5*, 1272−1277.

(26) Long, R.; Prezhdo, O. V. Instantaneous Generation of Charge-Separated State on TiO2 Surface Sensitized with Plasmonic Nanoparticles. *J. Am. Chem. Soc.* **2014**, *136*, 4343−4354.

(27) Chen, H.; McMahon, J. M.; Ratner, M. A.; Schatz, G. C. Classical Electrodynamics Coupled to Quantum Mechanics for Calculation of Molecular Optical Properties: A RT-TDDFT/FDTD Approach. *J. Phys. Chem. C* **2010**, *114*, 14384−14392.

(28) Lopata, K.; Neuhauser, D. Multiscale Maxwell−Schrödinger Modeling: A Split Field Finite-Difference Time-Domain Approach to Molecular Nanopolaritonics. *J. Chem. Phys.* **2009**, *130*, 104707.

(29) Sun, J.; Li, G.; Liang, W. How Does the Plasmonic Enhancement of Molecular Absorption Depend on the Energy Gap between Molecular Excitation and Plasmon Modes: A Mixed TDDFT/FDTD Investigation. *Phys. Chem. Chem. Phys.* **2015**, *17*, 16835−16845.

(30) Yam, C.; Meng, L.; Chen, G. H.; Chen, Q.; Wong, N. Multiscale Quantum Mechanics/Electromagnetics Simulation for Electronic Devices. *Phys. Chem. Chem. Phys.* **2011**, *13*, 14365−14369.

(31) Meng, L.; Yam, C.; Koo, S.; Chen, Q.; Wong, N.; Chen, G. H. Dynamic Multiscale Quantum Mechanics/Electromagnetics Simulation Method. *J. Chem. Theory Comput.* **2012**, *8*, 1190−1199.

DOI: 10.1021/acs.jpclett.5b01913
J. Phys. Chem. Lett. 2015, 6, 4410−4416

(32) Meng, L.; Yin, Z.; Yam, C.; Koo, S.; Chen, Q.; Wong, N.; Chen, G. Frequency-Domain Multiscale Quantum Mechanics/Electromagnetics Simulation Method. *J. Chem. Phys.* **2013**, *139*, 244111.
(33) Yam, C.; Meng, L.; Zhang, Y.; Chen, G. A Multiscale Quantum Mechanics/Electromagnetics Method for Device Simulations. *Chem. Soc. Rev.* **2015**, *44*, 1763−1776.
(34) Meuris, P.; Schoenmaker, W.; Magnus, W. Strategy for Electromagnetic Interconnect Modeling. *IEEE Trans. Comput.-Aided Design* **2001**, *20*, 753−762.
(35) Schoenmaker, W.; Meuris, P. Electromagnetic Interconnects and Passives Modeling: Software Implementation Issues. *IEEE Trans. Comput.-Aided Design* **2002**, *21*, 534−543.
(36) Ida, N.; Bastos, J. P. A. *Electromagnetics and Calculation of Fields*; Springer-Verlag: New York, 1997.
(37) Mur, G. Absorbing Boundary Conditions for the Finite-Difference Approximation of the Time-Domain Electromagnetic-Field Equations. *IEEE Trans. Electromagn. Compat.* **1981**, *EMC-23*, 377−382.
(38) Georgieva, N.; Yamashita, E. Time-Domain Vector-Potential Analysis of Transmission-Line Problems. *IEEE Trans. Microwave Theory Tech.* **1998**, *46*, 404−410.
(39) Zhang, Y.; Yam, C.; Chen, G. Dissipative Time-Dependent Quantum Transport Theory. *J. Chem. Phys.* **2013**, *138*, 164121.
(40) Lu, W.; Xiang, J.; Timko, B. P.; Wu, Y.; Lieber, C. M. One-Dimensional Hole Gas in Germanium/Silicon Nanowire Heterostructures. *Proc. Natl. Acad. Sci. U. S. A.* **2005**, *102*, 10046−10051.
(41) Zuloaga, J.; Prodan, E.; Nordlander, P. Quantum Description of the Plasmon Resonances of a Nanoparticle Dimer. *Nano Lett.* **2009**, *9*, 887−891.
(42) Esteban, R.; Borisov, A. G.; Nordlander, P.; Aizpurua, J. Bridging Quantum and Classical Plasmonics with a Quantum-Corrected Model. *Nat. Commun.* **2012**, *3*, 1806.
(43) Duan, H.; Fernández-Domínguez, A. I.; Bosman, M.; Maier, S. A.; Yang, J. K. W. Nanoplasmonics: Classical Down to the Nanometer Scale. *Nano Lett.* **2012**, *12*, 1683−1689.
(44) Johnson, P. B.; Christy, R. W. Optical Constants of the Noble Metals. *Phys. Rev. B* **1972**, *6*, 4370.
(45) Wu, Y.; Cui, Y.; Huynh, L.; Barrelet, C. J.; Bell, D. C.; Lieber, C. M. Controlled Growth and Structures of Molecular-Scale Silicon Nanowires. *Nano Lett.* **2004**, *4*, 433−436.
(46) Mirza, M. M.; MacLaren, D. A.; Samarelli, A.; Holmes, B. M.; Zhou, H.; Thoms, S.; MacIntyre, D.; Paul, D. J. Determining the Electronic Performance Limitations in Top-Down-Fabricated Si Nanowires with Mean Widths Down to 4 nm. *Nano Lett.* **2014**, *14*, 6056−6060.
(47) Sieck, A.; Frauenheim, T.; Pederson, M. R.; Jackson, K.; Porezag, D. Structure and Vibrational Spectra of Low-Energy Silicon Clusters. *Phys. Rev. A: At., Mol., Opt. Phys.* **1997**, *56*, 4890−4898.
(48) Frauenheim, T.; Seifert, G.; Elstner, M.; Niehaus, T.; Kohler, C.; Amkreutz, M.; Sternberg, M.; Hajnal, Z.; Di Carlo, A.; Suhai, S. Atomistic Simulations of Complex Materials: Ground-State and Excited-State Properties. *J. Phys.: Condens. Matter* **2002**, *14*, 3015−3047.
(49) Li, X.; Choy, W. C. H.; Lu, H.; Sha, W. E. I.; Ho, a. H. P. Efficiency Enhancement of Organic Solar Cells by Using Shape-Dependent Broadband Plasmonic Absorption in Metallic Nanoparticles. *Adv. Funct. Mater.* **2013**, *23*, 2728−2735.
(50) Klaus, G. *Metal Impurities in Silicon-Device Fabrication*; Springer-Verlag: Berlin/Heidelberg, 2000.
(51) Cuevas, A.; Kerr, M. J.; Samundsett, C.; Ferrazza, F.; Coletti, G. Millisecond Minority Carrier Lifetimes in N-Type Multicrystalline Silicon. *Appl. Phys. Lett.* **2002**, *81*, 4952−4954.
(52) Cotter, J. E.; Guo, J. H.; Cousins, P. J.; Abbott, M. D.; Chen, F. W.; Fisher, K. C. P-Type Versus N-Type Silicon Wafers: Prospects for High-Efficiency Commercial Silicon Solar Cells. *IEEE Trans. Electron Devices* **2006**, *53*, 1893−1901.

DOI: 10.1021/acs.jpclett.5b01913
J. Phys. Chem. Lett. 2015, 6, 4410−4416